Contents lists available at ScienceDirect

Journal of the Mechanical Behavior of Biomedical Materials

journal homepage: www.elsevier.com/locate/jmbbm

The effect of cortical thickness and thread profile dimensions on stress and strain in bone-anchored implants for amputation prostheses

Alexander Thesleff [a,b,c,*], Max Ortiz-Catalan [a,b,d,e], Rickard Brånemark [e,f]

[a] Center for Bionics and Pain Research, Göteborgsvägen 31, 431 80, Mölndal, Sweden
[b] Dept. of Electrical Engineering, Chalmers University of Technology, Hörsalsvägen 11, 412 58, Gothenburg, Sweden
[c] Integrum AB, Krokslätts Fabriker 50, 431 37, Mölndal, Sweden
[d] Operational Area 3, Sahlgrenska University Hospital, 431 30, Mölndal, Sweden
[e] Department of Orthopaedics, Institute of Clinical Sciences, Sahlgrenska Academy, University of Gothenburg, Sahlgrenska University Hospital, Göteborgsvägen 31, 431 80, Mölndal, Sweden
[f] Center for Extreme Bionics, Biomechatronics Group, MIT Media Lab, Massachusetts Institute of Technology, 77 Mass. Ave., E14/E15, Cambridge, MA, 02139-4307 USA, Cambridge, MA, USA

ARTICLE INFO

ABSTRACT

Skeletal attachment of limb prostheses ensures load transfer between the prosthetic leg and the skeleton. For individuals with lower limb amputation, these loads may be of substantial magnitude. To optimize the design of such systems, knowledge about the structural interplay between implant design features, dimensional changes, and material properties of the implant and the surrounding bone is needed. Here, we present the results from a parametric finite element investigation on a generic bone-anchored implant system of screw design, exposed to external loads corresponding to average and high ambulatory loading. Of the investigated parameters, cortical thickness had the largest effect on the stress and strain in the bone-anchored implant and in the cortical bone. 36%–44% reductions in maximum longitudinal stress in the bone-anchored implant was observed as a result of increased cortical thickness from 2 mm to 5 mm. A change in thread depth from 1.5 mm to 0.75 mm resulted in 20%–22% and 10%–18% reductions in maximum longitudinal stress in the bone-anchored implant at 2 mm and 5 mm cortical thickness respectively. The effect of changes in the thread root radius was less prominent, with 8% reduction in the maximum longitudinal stress in the bone-anchored implant being the largest observed effect, resulting from an increased thread root radius from 0.1 mm to 0.5 mm at a thread depth of 1.5 mm. Autologous transplantation of bone tissue distal to the fixture resulted in reductions in the longitudinal stress in the percutaneous abutment. The observed stress reduction of 10%–31% was dependent on the stiffness of the transplanted bone graft and the cortical thickness of surrounding bone. Results from this investigation may guide structural design optimization for bone-anchored implant systems for attachment of limb prostheses.

1. Background

For individuals with amputation, the socket-stump interface is the source of several commonly reported problems such as pain, pressure sores, skin problems, poor retention, and perspiration (Dudek et al., 2005; Hagberg and Brånemark, 2001; Hoaglund et al., 1983; Legro, 1999; Meulenbelt et al., 2011; Sherman, 1999). To address these issues, a method of bone-anchored attachment of limb prostheses was developed, where a surgically implanted percutaneous skeletal extension allows for direct attachment of the prosthesis (Brånemark et al., 2014). The method builds on the discovery that bone tissue may form an exceptionally intimate and mechanically stable connection with titanium (Branemark, 1983). This phenomenon is now known as osseointegration and is defined as "the firm anchoring of a surgical implant by the growth of bone around it without fibrous tissue formation at the interface" (Osseointegration, 2021). The first clinical applications of osseointegration were in the dental field, but it has since then spread to other applications such as hearing aids, facial reconstructions, and orthopaedic applications including bone-anchored attachment of prosthetic limbs (Brånemark et al., 2001). The method of bone-anchored attachment of prosthetic limbs was developed in Sweden with the first successful surgeries performed in 1990 (Eriksson and Brånemark, 1994).

* Corresponding author. Center for Bionics and Pain Research, Göteborgsvägen 31, 431 80, Mölndal, Sweden.
  E-mail addresses: thesleff@chalmers.se (A. Thesleff), maxo@chalmers.se (M. Ortiz-Catalan), rickardb@mit.edu (R. Brånemark).

A standardized implant system and treatment protocol was introduced in 1999 as the OPRA (Osseointegrated Prostheses for the Rehabilitation of Amputees) implant system (Integrum AB, Mölndal, Sweden). The OPRA implant system is CE-marked for transfemoral, transhumeral, and thumb/finger amputations, and custom-made implants are available for the aforementioned levels, as well as for transtibial and transradial amputations. Despite the required surgical intervention, rehabilitation, and the risk of infection due to the skin penetration, the treatment has gained increased clinical acceptance and is currently available in 14 countries. The OPRA implant system was recently granted a pre-market approval (PMA) by the Food and Drug Administration (FDA) in the USA for treatment at the transfemoral level. Following the successful clinical results of the OPRA implant system a few other systems for bone-anchored attachment of prosthetic limbs have been developed. Examples are the ILP (Integral Leg Prosthesis, ESKA Orthopaedic Handels GmbH, Germany) (also known as Endo-Exo Prosthesis (EEP)) and the OPL (Osseointegrated Prosthetic Limb, Permedica s.p.a., Italy). With bone-anchored attachment of the prosthesis, a socket is no longer needed and the aforementioned problems related to socket attachment are eliminated. Research on individuals who have undergone treatment with bone-anchored attachment of limb prosthesis shows that it may lead to improved quality of life, increase in prosthetic function and use, improved walking ability, walking efficiency, range of motion, sitting comfort, and sensory perception from the prosthesis via a phenomenon known as osseoperception (Al Muderis, 2016; Al Muderis et al., 2017; Clemente, 2017; Hagberg et al., 2005, 2014, 2020; Häggström et al., 2013; Jacobs et al., 2000; Tranberg et al., 2011; Van de Meent et al., 2013).

The OPRA implant system is a modular system, of which the structural components are the fixture and the abutment. The fixture is a cylindrical, externally threaded component, fully implanted into the residual bone. The abutment, which is the percutaneous component has its proximal end press-fitted into the fixture, and its distal end protruding out from the skin and allowing for attachment of the prosthesis. The rigid connection between the prosthesis and the skeleton may lead to a more efficient gait compared with the more compliant socket connection (Hagberg et al., 2014), (Van de Meent et al., 2013). However, it also means that any loads applied to the prosthesis are transferred directly to the bone-anchored implant and the periprosthetic bone which could be at risk of fracture. Several studies involving load cell measurements at the implant prosthesis interface have offered insights in the magnitude of the loading during ambulatory activities of daily living (Frossard, 2019; Lee, 2007a; Thesleff et al., 2020). This data is valuable for numerical simulations such as finite element (FE) analyses to calculate periprosthetic and implant stress and strain to quantify risk for fracture.

The objective of this study was to perform a parametric evaluation on the effect of thread profile parameters and cortical thickness on the peak stress and strains in a generic implant model subjected to external loads corresponding to average and high ambulatory loading. An additional aim was to quantify effects of changes in bone stiffness characteristics and distal bone resorption on the maximum stresses in the implant system. The generic model was inspired by the OPRA implant system; an externally threaded fixture and other components manufactured from medical grade titanium (Ti6Al4V). The intention was to provide knowledge on how the careful selection of design features can minimize the risk of bone or implant fracture during use. This study contrasts earlier FE-based studies which have been either case studies with subject specific anatomy (Elder et al., 2017; Prochor and Sajewicz, 2019a,b, Tomaszewski et al., 2012a,a,b, Xu et al., 2006, 2016), studies focused exclusively on bone remodelling around the implant (Prochor and Sajewicz, 2019a), (Prochor et al., 2020), or FE-implementations with too low resolution to accurately capture the stress in the threaded region (Elder et al., 2017; Helgason et al., 2009; Lee, 2007b; Prochor and Sajewicz, 2019b; Tomaszewski et al., 2012a,b,b, Xu et al., 2000, 2006, 2016).

2. Method

2.1. Geometry

The generic model used in this study is shown in Fig. 1. The geometrical parameters that we investigated were thread depth (d), thread root radius (r_{root}), and the cortical thickness (t) within the parameter space shown in Fig. 1. The thread depth is inversely related in the core diameter of the fixture whereas the thread root radius influences the stress concentration in the thread roots of the fixture. These parameters were therefore anticipated to have a large influence on the peak stress and strains in the bone-anchored implant system in the evaluated load scenarios. The fixture thread was a standard V-shaped thread with 30° flank angle, a rounded thread crest with constant radius of 0.1 mm and either a small or a large root radius, of 0.1 mm or 0.5 mm, respectively. Three thread depths were evaluated 0.75 mm, 1.125 mm and 1.5 mm. The thread pitch (p) was determined by the thread depth, where a larger thread depth led to a larger pitch. It was kept constant for each thread depth, regardless the value of root radius to discern the effect of this parameter. Two cortical thicknesses were evaluated, a small cortical thickness of 2 mm which correspond to the minimum requirement after implantation according to the OPRA surgical protocol (Li and Lindeque, 2018), and a larger cortical thickness of 5 mm.

2.2. Analytical estimation of load sharing

Prior to performing the FE-simulations, an analytical analysis was performed on a simplified geometry, considering the implant and the cortical bone as two uniform cylinders (without threads) with dimensions as indicated in Fig. 1. In this analysis both the Ti6Al4V and the cortical bone were assumed to have isotropic properties with Young's modulus of 110 GPa and 17 GPa, respectively. Assuming a pure bending load case and disregarding shear forces at the interface between the cylinders, the analytical load sharing between the implant and the cortical bone was calculated based on respective component's bending stiffness, defined as the product of Young's modulus, (E), and the area moment of inertia according, (I), according to Eq. (1), with (d_o) and (d_i) being the external and internal diameter respectively.

$$EI = E\frac{\pi}{64}\left(d_o^4 - d_i^4\right) \tag{1}$$

This initial investigation was conducted with the purpose to serve as a point of reference for the FE-simulation results.

2.3. FE-model

FE-modelling and simulations were performed using COMSOL Multiphysics version 5.5 (Comsol AB, Sweden). A generic 3D axisymmetric model of the implant system and surrounding bone was created where the symmetry in geometry allowed for reduction of the model to half of the full geometry (Fig. 1). The abutment and fixture were combined into a single component. In accordance with the surgical protocol of the OPRA implant system, the fixture was countersunk 20 mm into the cortical bone with the distal void filled with a less stiff autologous bone transplant (Stenlund et al., 2016), (Hoyt et al., 2020). The interfaces between fixture and the cortical bone and between fixture and transplanted bone were modelled with shared nodes, assuming full osseointegration, (which is close to what has been observed from histological assessment of a retrieved fixture (Palmquist et al., 2014)), whereas the interface between the abutment and the transplanted bone was modelled assuming no osseointegration and frictionless sliding. The cortical bone extended 20 mm distally and proximally from both ends of the fixture. The proximal end of the cortical bone was constrained in all degrees of freedom. The external load was applied at the distal end of the abutment as a static load case.

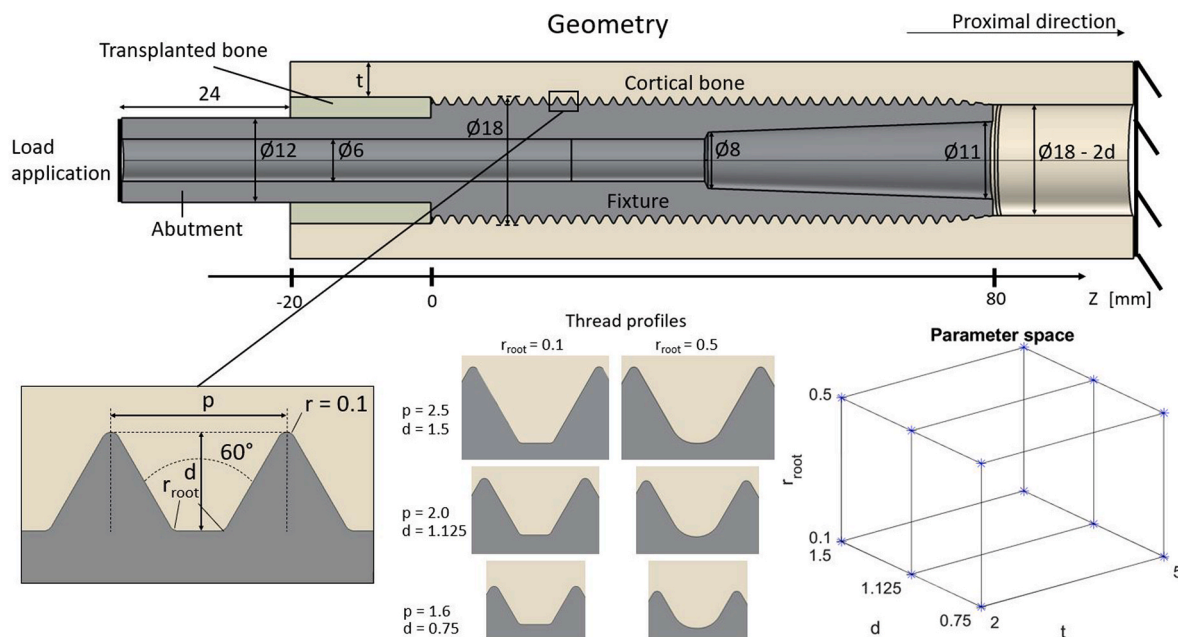To meet computational limitations in the hardware while ensuring a

Fig. 1. Generic geometry with boundary conditions and dimensions. Dimensions denoted with variable names were varied within the study, whereas dimensions with numerical values were fixed. At the bottom right the evaluated parameter space is shown with the individual analysis points indicated with blue asterisks.

sufficiently dense mesh along the full geometry of the threaded implant, a stepwise submodelling scheme was employed (Fig. 2). A global model with the full model geometry was created, transversely partitioned at locations indicated in Fig. 2. Subsequently, five densely meshed submodels were created. Global model simulation results (displacements)

at the partition surfaces were applied as boundary conditions (prescribed displacement) at the corresponding surfaces in the submodels to generate high resolution simulation results for each of the submodels. Simulation results along longitudinal evaluation profiles in each of the submodels were exported from COMSOL and imported into Matlab
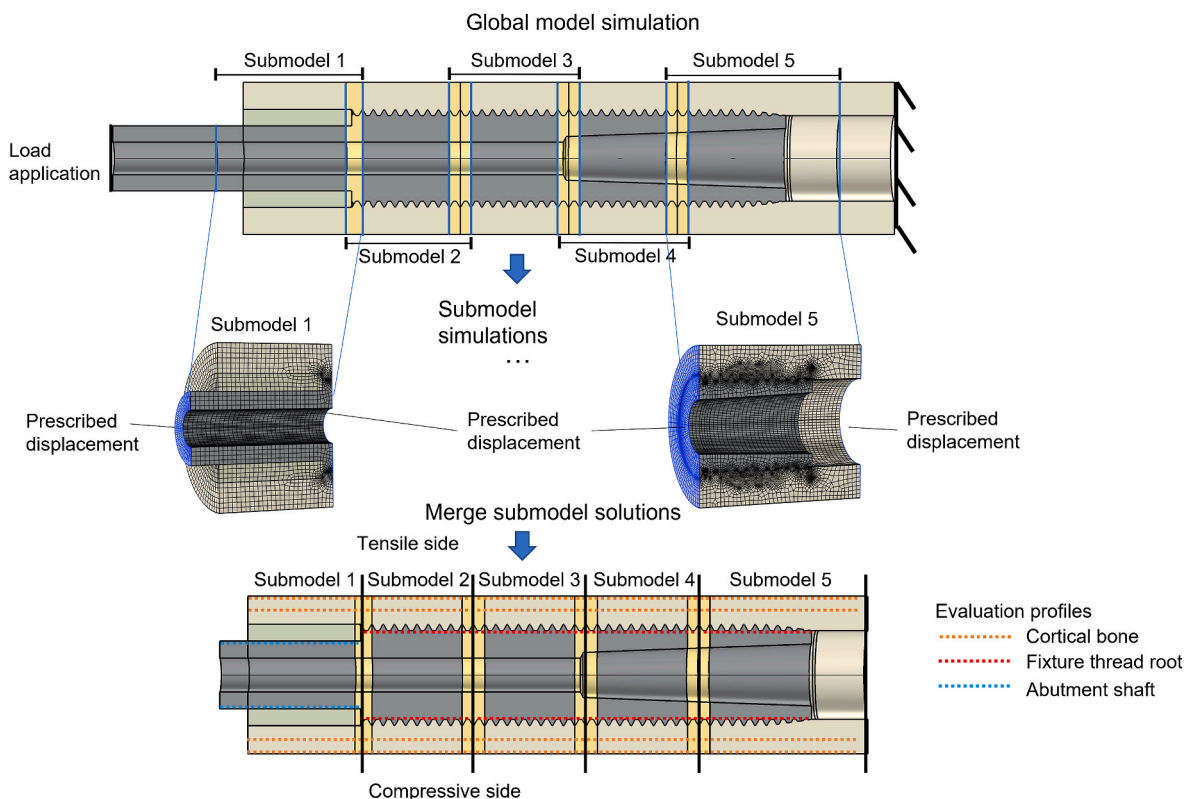

Fig. 2. Simulation scheme using submodelling. Top. Global model with submodel partitions. Yellow segments indicate overlapping regions which were included in both neighbouring submodels. Middle. Densely meshed submodels. Blue surfaces show where prescribed displacement was assigned from corresponding surfaces in the global model (indicated with blue lines in top image). Bottom. Merging results from each submodel simulation and plotting results along the longitudinal direction at the indicated evaluation profiles.

(version 2019a, MathWorks Inc., Natick, MA, USA). Custom written scripts were used to integrate the results between the submodels and to visualize the results along the combined evaluation profiles. To avoid non-physical stress singularities at the border of the submodels due to mesh size inconsistencies between the submodels and the global model, a small overlap was included between the neighbouring sub-models (yellow regions in Fig. 2). In the data processing stage, the exported simulation results close to the longitudinal end points of the sub-model were discarded so that each submodel only contributed with simulation results starting from the centre of the overlapping zone. In addition to eliminating singularities at the submodel borders, this ensured that no duplicate data was used to form the combined simulation results.

2.4. Material properties

The material models and material properties used in the simulations are presented in Table 1. Transverse isotropy was assumed for the cortical bone, with uniform material properties around the longitudinal axis. Young's and shear moduli were obtained from the investigation by Reilly and Burstein (1975) where the transversely isotropic material properties had been determined based on experimental measurements on human cadaver femora. Single case simulations with the longitudinal Young's modulus of the cortical bone reduced to 12 GPa were also performed. This reduced stiffness may arise due to increased porosity of the cortical bone tissue, which is a natural consequence of aging, osteoporosis, and not loading the skeleton in a physiological way, an example being individuals with a lower limb amputation fitted with a socket prosthesis (Bemben et al., 2017; Sherk et al., 2008; Zioupos and Currey, 1998). The reduction of the longitudinal Young's modulus from 17 GPa to 12 GPa was determined based on experimental data from a study by Dong and Guo (2004) where the aforementioned values corresponded to cortical porosity of 8.5% and 19% respectively. An additional case of reduced bone support was simulated corresponding to an extreme case of distal resorption, modelled by removing the transplanted bone and the 40 mm most distal portion of the cortical bone. Two versions of transplanted bone were evaluated, immature transplanted bone with a low Young's modulus representing the state during early rehabilitation, and mature transplanted bone with a higher Young's modulus representing the steady state after full healing and rehabilitation has taken place. Prior histological observation of a tissue biopsy of the transplanted bone retrieved from a revision surgery of an OPRA implant system showed that the mature transplanted bone obtained a trabecular bone structure with a compact bone layer towards the soft tissue and the abutment (Stenlund et al., 2016). For simplicity, the transplanted bone was modelled as a homogeneous isotropic tissue with values on the material properties selected to be identical to those previously used by Stenlund et al. (2016). The fixture and the abutment

Table 1
Material models and material properties used in the FE-models.

Component	Material model	Material properties
Fixture and abutment	Linear elastic Isotropic	$E = 110$ GPa $\nu = 0.3$
Normal cortical bone	Linear elastic Transversely isotropic	$E_r = E_\Theta = 11.5$ GPa, $E_z = 17$ GPa $G_{r\Theta} = 3.6$ GPa, $G_{rz} = G_{\Theta z}$ 3.3 GPa $\nu_{r\Theta} = \nu_{rz} = \nu_{\Theta z} = 0.3$
Osteoporotic cortical bone	Linear elastic Transversely isotropic	$E_r = E_\Theta = 11.5$ GPa, $E_z = 12$ GPa $G_{r\Theta} = 3.6$ GPa, $G_{rz} = G_{\Theta z}$ 3.3 GPa $\nu_{r\Theta} = \nu_{rz} = \nu_{\Theta z} = 0.3$
Mature transplanted bone	Linear elastic Isotropic	$E = 4$ GPa $\nu = 0.3$
Immature transplanted bone	Linear elastic Isotropic	$E = 0.4$ GPa $\nu = 0.3$

Table 2
Investigated load cases. F denotes longitudinal force. M denotes bending moment.

Load case	F [N]	M [Nm]	Interpretation
LC1	1000	90	High ambulatory loading
LC2	625	37	Average ambulatory loading

are manufactured from Ti6Al4V and were also modelled with isotropic material properties.

2.5. Load cases

From studies obtaining direct load data at distal end of the abutment, it is known that at physiological loading during activities of daily living, the bending moment is the main contributor to the stress state in the implant and the bone, and that the longitudinal force is the dominating force component (Thesleff et al., 2020). The studied load cases (see Table 2) were therefore reduced to only include these components. This led to symmetric loading which in combination with the geometric symmetry allowed for the model reduction as described above. The first load case, LC1, refers to high loading ambulation. The highest body weight acceptable for treatment with the OPRA implant system is 100 kg. During walking this corresponds to a maximum longitudinal force, of approximately 1000 N. This value was therefore chosen for the longitudinal force component, **F**, for LC1. The bending moment was derived from a study conducting load measurements at the distal end of the abutment in 20 individuals with the OPRA implant system at the transfemoral level while performing everyday ambulatory activities (Thesleff et al., 2020). The highest measured bending moment reported during any of the investigated activities within that study was 90 Nm (observed in a single participant during stairs descent). This value was therefore chosen as the value for the bending moment, **M**, in LC1. The second load case, LC2, refers to average loading during level ground walking. The magnitudes of the longitudinal force and the bending moment were also derived from the aforementioned study. They correspond to the mean peak longitudinal force and mean peak bending moment measured across the study participants during level ground walking. A simulation log specifying all evaluated parameters and load cases is provided as supplementary data.

The FE meshes of both the global model and the submodels were created by first creating a structured surface mesh on a longitudinal section of the axisymmetric FE-geometry. The surface mesh was refined in the threaded portion of the geometry. The surface mesh was then swept around the longitudinal axis to form a 3D mesh. This meshing strategy was chosen to minimize the number of elements in the model while ensuring a high mesh resolution in the threaded region. The resulting mesh consisted of second order hexahedron and prismatic elements. The total number of elements were 90 000–120 000 for the global models and 35 000–80 000 for each sub-model depending on variations in geometry (i.e., variations in t, r_{root}, d, and p). A mesh convergence analysis along a longitudinal profile along the fixture thread root, the region most influenced by the quality of the mesh, confirmed that further mesh refinement from the chosen mesh parameters led to <3% change in results anywhere along the profile (see supplementary data for details).

3. Results

LC1 and LC2 both correspond to repeated loading conditions for which tensile stresses in general are considered more harmful than compressive stresses (Dowling, 2007). For this reason, only the stress and strain state on the tensile side of the implant-bone model is reported in this study.

3.1. Analytical estimation of load sharing

The result from the analysis of the simplified geometry, considering the implant and the cortical bone as two uniform cylinders is shown in Fig. 3.

3.2. Stress in fixture

Thread roots constitute stress concentrations with locally elevated stress levels (Shigley et al., 2002). The thread root of the fixture may therefore be susceptible to high stress levels and could be a potential location of failure if exposed to excessive loading. Tensile and compressive stresses are given by the longitudinal stress component. The longitudinal stress in the thread root of the tensile side of the fixture subjected to LC1 is presented in Fig. 4 for three different thread depths and for two different cortical thicknesses.

At the distal end of the fixture, (z = 0), the peak stresses are reduced in all studied cases. This is also observed at the proximal end of the fixture for the cases with the large cortical thickness, (t = 5 mm). However, for the case with small cortical thickness (t = 2 mm), there is an increase in the peak stress in the fixture towards the proximal end especially for the two more shallow thread depths with a small thread root radius. Between the z-coordinates, 20 mm and 60 mm along the fixture, the differences between the peak stress profiles are approximately constant, thus the effect of each parameter can be approximated by an average over this region without losing much detail. Such summarized presentation of the parameter evaluation is shown in Fig. 5.

Within the investigated parameter space, the difference between 2 mm and 5 mm cortical thickness had the largest effect on the peak stresses in the fixture thread root, with approximately 40% reduction across different thread depths and root radii. A reduced thread depth from 1.5 mm to 0.75 mm led to 20–22% reduction with t = 2 mm and 10–18% reduction with t = 5 mm. The effect of an increased radius in the thread root from 0.1 mm to 0.5 mm had a less prominent effect, and stress reductions were only noted for the most deep and shallow threads at t = 2 mm (Fig. 6) and the deepest thread at t = 5 mm. In the three other simulated cases, no change in the average peak stress was noted.

The separate effects of reduced cortical stiffness and extreme distal bone resorption on the maximum stress in the thread root of the fixture are shown in Fig. 7. On average, a reduction in the longitudinal cortical stiffness from 17 GPa to 12 GPa resulted in 12% and 30% increases in maximum longitudinal stress for 2 mm and 5 mm cortical thickness,
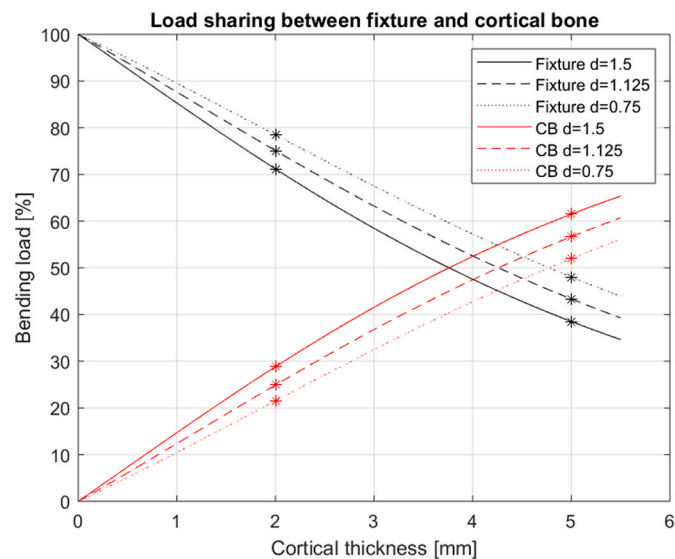
respectively. In the case of extreme bone resorption, the maximum stress increased by 54% on average compared with a situation of full uniform cortical bone support (t = 2 mm).

3.3. Stress in abutment

A comparison of the longitudinal stress on the tensile side of the abutment shaft for different configurations of cortical thickness and Young's modulus for the transplanted bone is presented in Fig. 8. With respect to the case without any bone support (extreme distal bone resorption) a maximum stress reduction of 31% was achieved with 5 mm cortical thickness and a Young's modulus of 4 GPa in the transplanted bone. Interestingly, even the smallest cortical thickness (t = 2 mm) and a very soft transplanted bone (E_{TB} = 0.4 GPa) resulted in up to 10% reduction in the stress of the abutment.

3.4. Stress and strain in cortical bone

The longitudinal stress and strain along the tensile side of the cortical bone is shown in Fig. 9. To show the effect of the cortical thickness and the cortical stiffness, all graphs presented in Fig. 10 are from simulations with fixed thread depth d = 1.125 mm and fixed thread root radius r_{root} = 0.5 mm. There were clear maxima in the longitudinal stress and longitudinal strain at the z-coordinates corresponding to each end of the fixture. Especially large were the maxima at the proximal end for the simulated cases with 2 mm cortical thickness. At the outer cortex at this location the maximum longitudinal stress reached 109 MPa and 43 MPa for LC1 and LC2 respectively for the simulations with ordinary cortical stiffness ($E_{L\ CB}$ = 17 GPa). For the 5 mm cortical thickness cases the maximum stress was 43 MPa at the outer cortex. At the distal end of the fixture the maximum stress in the cortical bone reached at most 42 MPa and 27 MPa for the simulations with 2 mm and 5 mm cortical thickness, respectively.

As a natural consequence of Hooke's law, a reduction of the cortical stiffness led to reduced stress but increased strains. The strains at the proximal end of the fixture were the largest, locally reaching 7940 με for the softer cortical bone simulation and 6050 με for the normal cortical bone simulation with 2 mm bone thickness in LC1. In LC2 the peak strain reached 2370 με with ordinary cortical bone stiffness.

In Fig. 10, the effect of the thread profile parameters, d and r_{root} on the longitudinal stress and longitudinal strain in the cortical bone is shown. The presented graphs are both from LC1 and at cortical thickness t = 2 mm. At the outer cortex along the length of the fixture, higher stress and strains are observed for the simulations with large thread depth, except for locations corresponding to the ends of the fixture. At the z-coordinate corresponding to the proximal end of the fixture longitudinal stress and longitudinal strain is lower in simulations with large thread depth. The highest values for the longitudinal stress and longitudinal strain in the cortical bone were observed at the proximal end of the fixture for the shallowest thread depth and the smallest fixture thread root radius and smallest cortical thickness.

4. Discussion

We conducted an FE-based evaluation of a generic model of a bone-anchored implant system inspired by the OPRA implant system that was subjected to external loads corresponding to average and high ambulatory loading. Within this investigation, a parametric analysis has been carried out to determine how the peak stress and strains in the implant system and the periprosthetic bone are affected by the cortical thickness, the thread depth, and the thread root radius. Single case investigations have been performed to quantify the effects of reduced cortical stiffness and distal bone resorption.
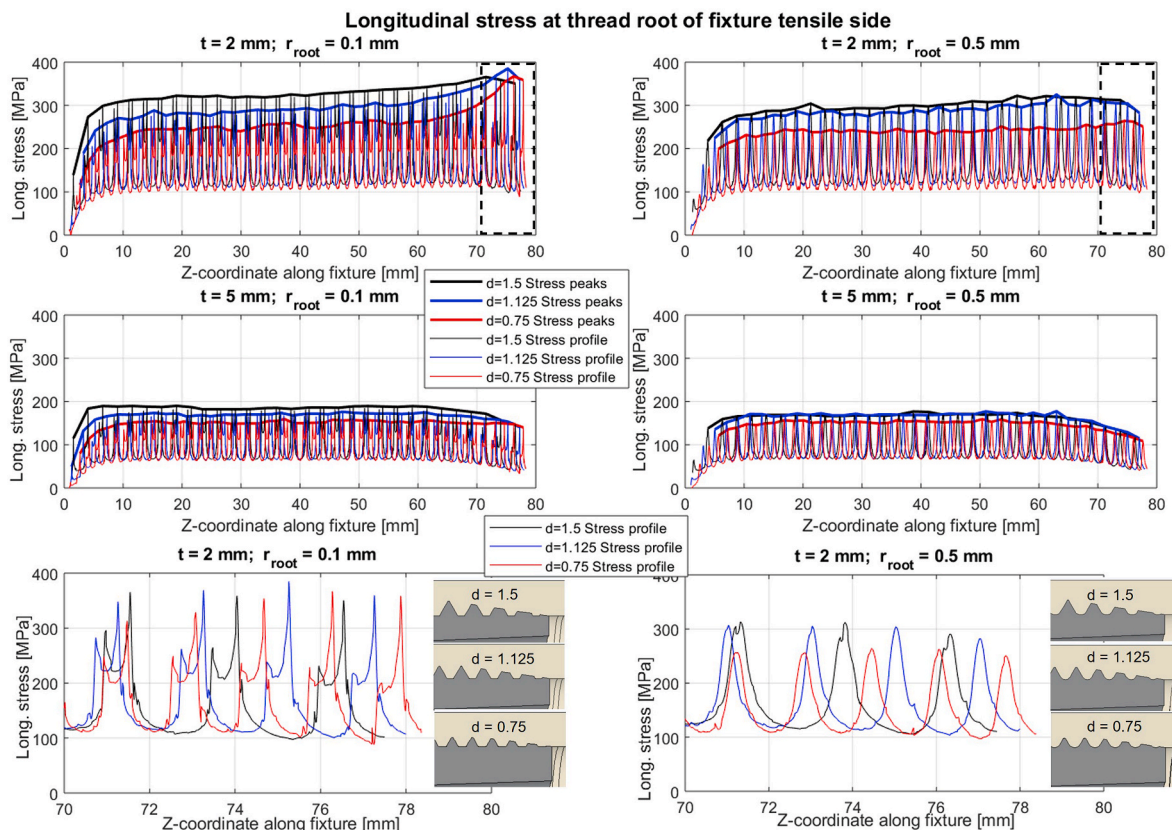

Fig. 3. Estimated load sharing between fixture and cortical bone (CB) from analysis of simplified geometry.

Fig. 4. Longitudinal stress in tensile side of the fixture thread root during LC1. Top. Results from simulations of three different values of the thread depth, d. Cortical thickness, t, and fixture thread root radius, r_{root} are kept constant at 2 mm and 0.5 mm respectively. Middle. Results from simulations of three different values of the thread depth, d. Cortical thickness, t, and fixture thread root radius, r_{root} are kept constant at 5 mm and 0.5 mm, respectively. Bottom. Results from the proximal end of the fixture with cortical thickness t = 2 mm (zoomed in from the dashed regions within the top graphs). The proximal geometry of the fixture is also shown.
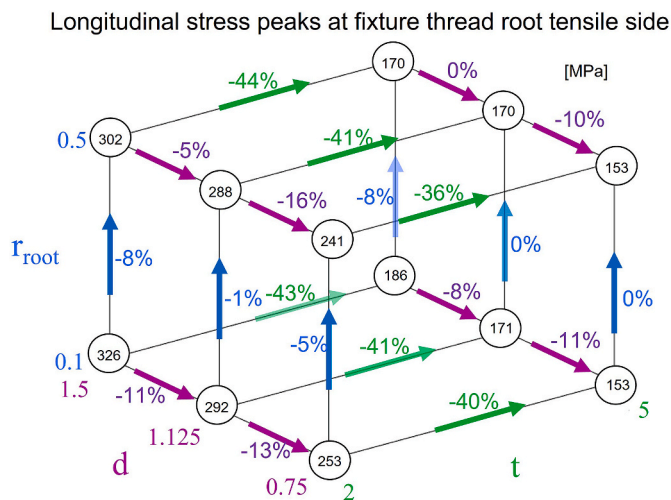

Fig. 5. Parameter evaluation of the longitudinal stress in the thread root of the fixture during LC1. Circled values denote the average peak longitudinal stress (MPa) in the fixture thread root between z-coordinates 20 mm and 60 mm during LC1. Coloured values denote the percentage difference in the results when varying a parameter.

4.1. Stress in fixture

The initial analytical approximation of the cortical bone and the fixture as two cylindrical components without thread provided preliminary predictions for the results from the FE-simulations. Changes in cortical thickness and thread depth, each lead to changes in the external diameter of respective component. Changes in the cortical thickness had the largest effect on the longitudinal stresses in the thread root of the fixture. This was expected considering the external diameter's high influence on the area moment of inertia (Eq. (1)). The average reductions of the peak longitudinal stress in the thread root of the fixture, when increasing the cortical thickness from 2 mm to 5 mm, were similar between the FE-simulations (36%–44%) and the predicted values (39%–46%).

The effect of the thread depth was influenced by the cortical thickness. With cortical thickness fixed at t = 2 mm, reducing the thread depth from 1.5 mm to 0.75 mm, led to 20% and 22% reduction in the average peak stress in the thread root of the fixture with a large and small root radius respectively. With cortical thickness fixed at t = 5 mm, the effect of an identical reduction in thread depth (1.5 mm–0.75 mm), led to smaller reductions (10% and 18% for large and small root radius respectively). The reason for the smaller influence of the thread depth at the larger cortical thickness can be attributed to the same reason as described above, namely the external diameter's importance for the bending stiffness (Eq. (1)).

Interestingly, for a cortical thickness of 2 mm and a small root radius, the magnitude of the stress peaks increased towards the proximal end of the fixture for the two shallower threads (Fig. 4). At the proximal end of the fixture the internal diameter of the fixture was 11 mm for all models whereas the external diameter of the fixture was dependent on the thread depth (Fig. 1). As a result, the external diameter and material thickness of the fixture was larger for models with smaller thread depth. This led to that the proximal stiffness of the fixture was larger in models with small thread depth. It also led to a smaller proximal stiffness reduction of the fixture (due to the chamfered external diameter
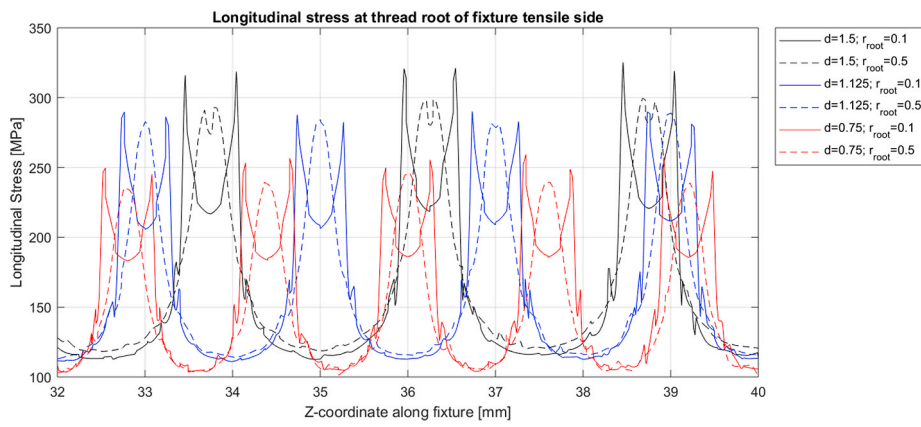
Fig. 6. Longitudinal stress in tensile side of the fixture thread root during LC1 for different thread depths and thread root radii. The cortical thickness is 2 mm in all graphs in the figure.
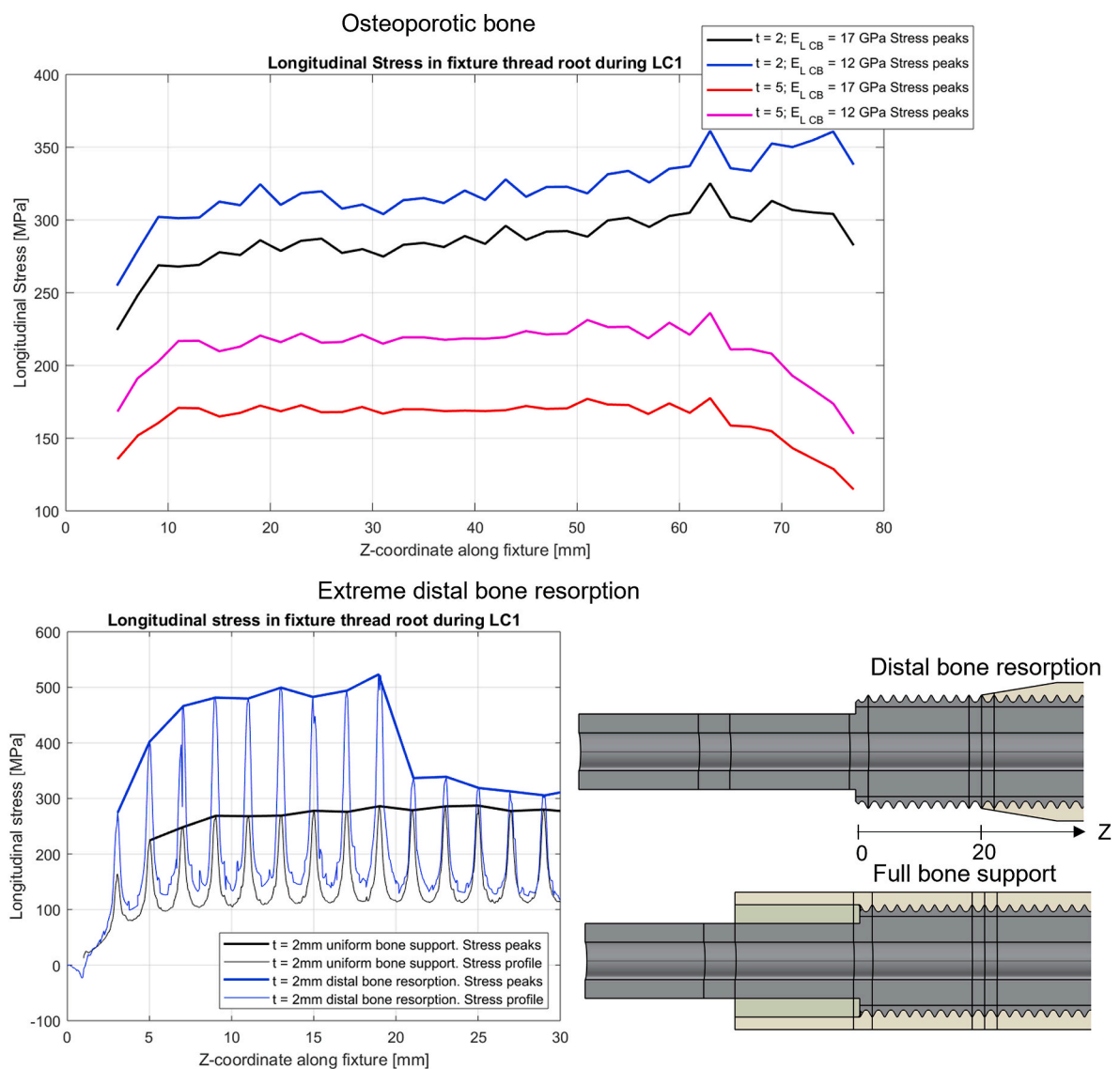

Fig. 7. Top. The longitudinal stress peaks in the fixture thread root for two different values of longitudinal stiffness in the cortical bone and for two different cortical thicknesses during LC1. Bottom. The effect of extreme distal bone resorption during LC1.
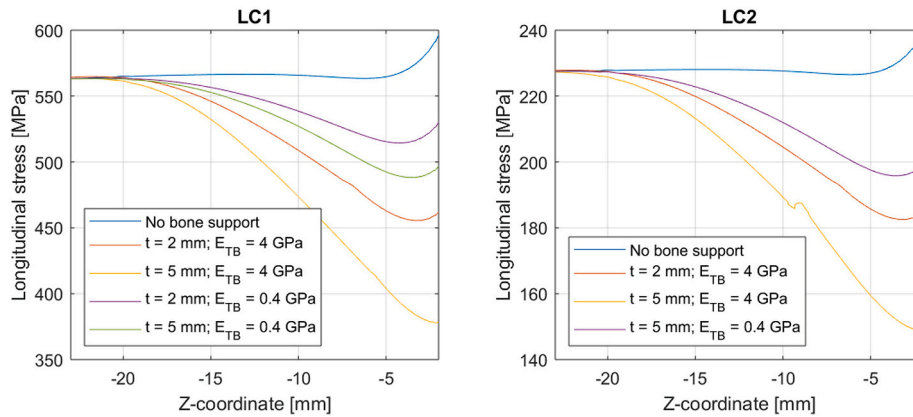
Fig. 8. Longitudinal stress on the tensile side of the abutment shaft during LC1 and LC2.
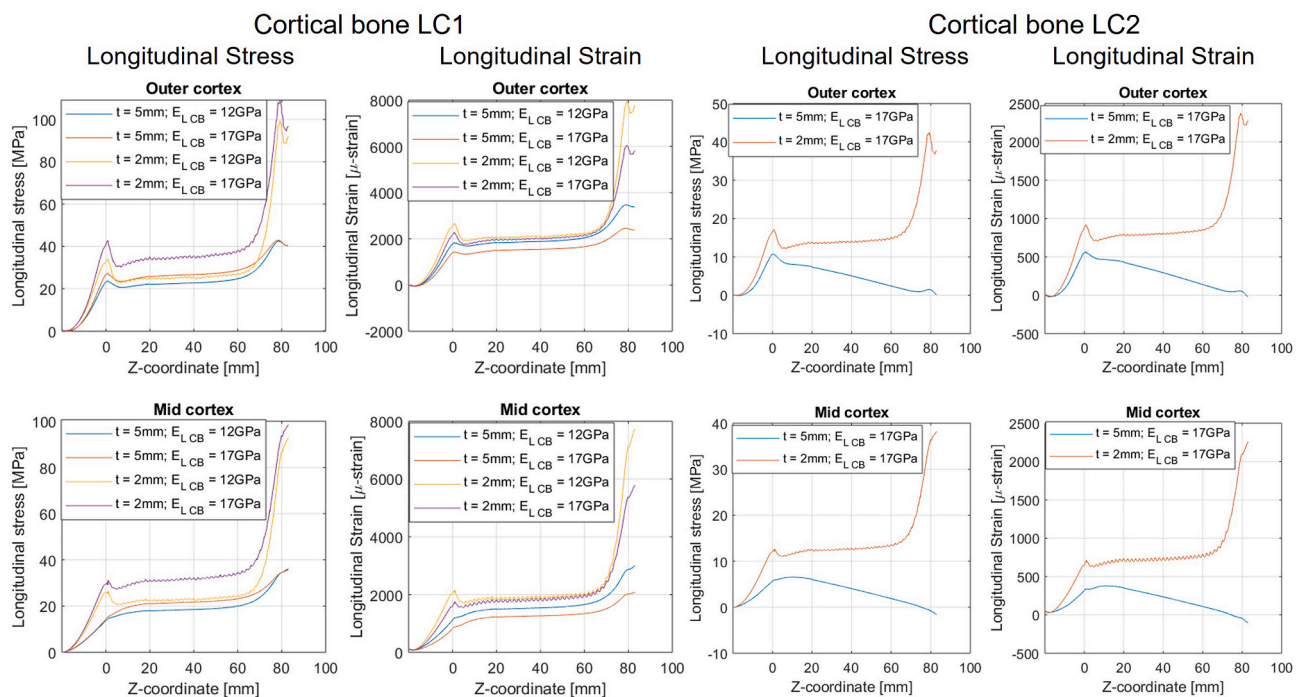

Fig. 9. Longitudinal stress and strain in the cortical bone during LC1 and LC2. For the results presented in the graphs the parameters d, and r_{root}, were kept fixed at 1.125 mm and 0.5 mm respectively.

proximally) in these FE-models. This may offer one explanation for the observed increased peak stress at the thread root of the proximal fixture for the shallower threads at 2 mm cortical thickness in Fig. 4.

The effect of reduced cortical stiffness was larger for the situation with large cortical thickness, since in this case the cortical bone is resisting a larger portion of the total load and thus a reduction in stiffness consequently has a larger effect on the stresses in the Fixture (Eq. (1)). The simulation with extreme distal bone resorption led to a 54% increase in the peak stresses in the fixture thread root compared with the reference case with uniform bone support with 2 mm cortical thickness. Such increase in the stresses might challenge the mechanical integrity of the fixture and thus, the resorption should be addressed before reaching such extremes.

4.2. Stress in abutment

The stress in the abutment was higher than the stress in the fixture,

an effect of the smaller external diameter and the conscious design decision to make the abutment the weaker component, since it can be more easily replaced if damaged than the fully implanted and osseointegrated fixture. The simulations showed that the transplanted bone can contribute to substantial stress reductions in the abutment, especially proximally corresponding to the region where the abutment exits from the fixture and would otherwise be particularly vulnerable. The transplanted bone bridges the gap between the distal cortical bone and the abutment and thus the cortical bone may contribute to resisting the bending loads. The advantage of the transplanted bone was observed with material properties representing immature transplanted bone and improved as the stiffness increased.

4.3. Stress and strain in cortical bone

With minimum cortical thickness (2 mm), the maximum longitudinal stress reached above 100 MPa at the outer cortex at the level of the
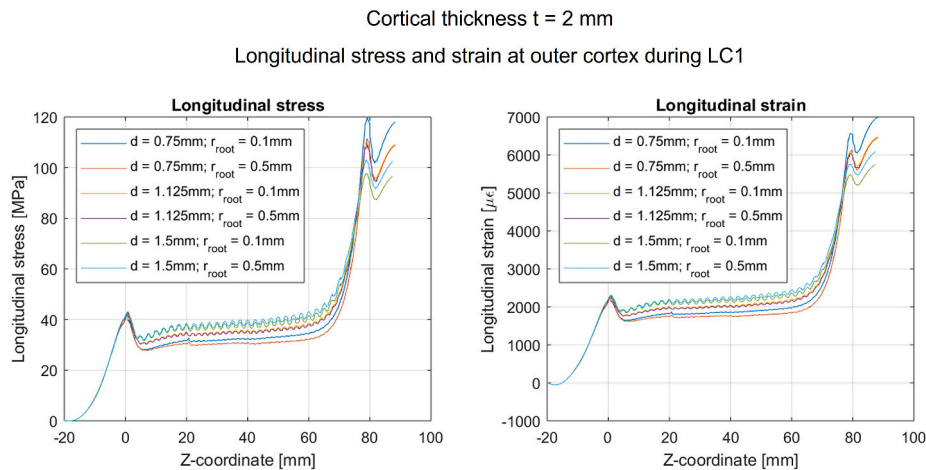
Cortical thickness t = 2 mm

Longitudinal stress and strain at outer cortex during LC1

Fig. 10. Longitudinal stress and strain during LC1. The parameter t is kept constant at 2 mm in the graphs.

proximal end of the fixture during LC1. For the 5 mm cortical thickness cases, the maximum stress was 43 MPa. At the distal end of the fixture the peak stress in the cortical bone reached at most 42 MPa for the case with 2 mm cortical thickness. For LC2 loading, the maximum stress reached 42 MPa at the level of the proximal end of the fixture. A reduction of the cortical stiffness led to reduced stress but increased strains. The strains at the proximal end of the fixture were the largest, locally reaching up to 8000 με for the softer cortical bone simulation and around 6000 με for the normal cortical bone simulation with 2 mm bone thickness in LC1 (Fig. 4). These strain levels are in the order of the yield strain reported from previous research (Wolfram and Schwiedrzik, 2016). In the FE-simulations, a small thread depth led to higher peak longitudinal stress and longitudinal strain in the cortical bone at to the proximal end of the fixture compared with a larger thread depth (Fig. 10). This may be explained by the fact that a smaller thread depth led to reduced proximal cortical bone thickness due to its geometrical definition in the FE-models as t + d (Fig. 1). Along the fixture length between the local maxima at each end of the fixture, higher longitudinal stress and longitudinal strains were instead observed for the simulations with large thread depth. This may be explained by the fact that the fixtures with larger thread depth provide less stress shielding of the bone due to their smaller core diameter, thereby leading to increased strains and stresses in the cortical bone.

For LC2 the peak strain was 2370 με for cortical bone with ordinary stiffness and 2 mm cortical thickness. For the case with 5 mm cortical thickness there were only minor local stress and strain peaks at the location of the proximal end of the fixture. It has been suggested that peak longitudinal strains above 1000 με leads to endosteal and periosteal bone formation but little change intracortically, whereas peak longitudinal strains below 1000 με leads to bone loss due to endosteal resorption and increased intracortical porosity (Rubin and Lanyon, 1985). This would suggest that during both LC1 and LC2 new bone formation at the proximal end of the fixture is to be expected, at least locally in the plane which is subjected to the highest bending moment. This would lead to an increased cortical thickness with subsequent, local decrease in stress and strain and a reduced risk of periprosthetic fracture in case of overloading.

4.4. Limitations

There are discrepancies between the geometry of FE-model and the clinically used implant system. As mentioned above, the proximal stiffness reduction of the fixture was not uniform between models of different thread depths. This led to that especially the FE-models with shallow thread depths had unrealistically high stiffness proximally. Furthermore, the FE-models lacked longitudinal slots in the proximal

fixture, a feature present in the clinically used fixtures. Slots act to reduce proximal stiffness and therefore, it can be assumed that the stress and strain concentrations in the cortical bone at the proximal end of the fixture are more severe in the FE-model compared with the clinically used implant. A detailed investigation of the effect of the proximal fixture stiffness on the stress and strain in the cortical bone at the proximal end of the fixture was outside the scope of this evaluation and would require a separate study. Another difference between the FE-geometry and the clinically used implant system is that the fixture and abutment were modelled as a single component rather than as separate components, thus omitting any effects from the interference fit at the contacting interface. Furthermore, the abutment screw and the preload were disregarded in the FE-model. This led to the omission of the resulting compressive stresses in the abutment shaft and thus, the presented longitudinal stress on the tensile side of the abutment shaft may be exaggerated by approximately 50 MPa compared with the clinical scenario. The geometry of the bone was modelled as a cylinder with uniform external diameter with the implant concentrically placed within the bone. This is a simplification from individual clinical cases which may vary both in the bone geometry and the implant placement. The load cases used in this study were derived from *in vivo* experimentally measured longitudinal forces and bending moments, but no torsional load components were considered. Furthermore, the variability in loading between users is known to be large (Thesleff et al., 2020), thus the magnitudes of the forces and moments may not be applicable to describe any individual user.

5. Conclusion

We conducted a numerical simulation (FE) of a bone-anchoring implant system. We found that the cortical thickness had the largest effect on stress and strain in the cortical bone and the fixture. At loads corresponding to high loading ambulation, 5 mm of cortical bone thickness led to approximately 40% lower maximum longitudinal stresses at the central half of the fixture compared with a cortical thickness of 2 mm. Changes within the investigated range of thread profile parameters had a smaller effect (0–8% stress reduction for a thread root radius of 0.5 mm as compared with 0.1 mm, and 10–22% stress reduction for thread depth of 0.75 mm as compared to 1.5 mm). At the location where the abutment exits from the fixture, autologously transplanted bone may provide substantial support for the abutment by activating support from surrounding cortical bone. We observed 10% and 31% stress reduction in the abutment for simulations with transplanted bone with Young's modulus of 0.4 GPa and 4 GPa, respectively. Reduced cortical bone stiffness led to increased stresses in the fixture. A 29% reduction in the longitudinal Young's modulus of the cortical bone

led to a 12% and 30% increase in maximum stress in the fixture at cortical thickness 2 mm and 5 mm, respectively. If distal bone resorption would occur to the extent that a portion of the distal fixture is without support from cortical bone, the maximum stress in the fixture may increase by up to 54% as compared with full cortical support of 2 mm cortical thickness.

The results from this investigation provide quantitative information on the interplay between geometrical and material parameters of the implant system and surrounding bone, and their effects on the stress and strain in respective material. This may inform further development of implant systems for bone-anchored attachment of limb prostheses.

Funding

CRediT authorship contribution statement

Alexander Thesleff: Conceptualization, Formal analysis, Methodology, Writing – original draft, Writing – review & editing. **Max Ortiz-Catalan:** Writing – review & editing. **Rickard Brånemark:** Conceptualization, Writing – review & editing.

Declaration of competing interest

The authors declare the following financial interests/personal relationships which may be considered as potential competing interestsAlexander Thesleff reports a relationship with Integrum AB that includes: employment and equity or stocks. Max Ortiz-Catalan reports a relationship with Integrum AB that includes: consulting or advisory and equity or stocks. Rickard Branemark reports a relationship with Integrum AB that includes: board membership and equity or stocks.

Appendix A. Supplementary data

Supplementary data to this article can be found online at https://doi.org/10.1016/j.jmbbm.2022.105148.

References

Al Muderis, M., Lu, W., Li, J.J., 2017. Osseointegrated Prosthetic Limb for the treatment of lower limb amputations : experience and outcomes. Unfallchirurg 120 (4), 306–311.
Al Muderis, M., et al., 2016. The Osseointegration Group of Australia Accelerated Protocol (OGAAP-1) for two-stage osseointegrated reconstruction of amputated limbs. Bone Joint Lett. J 98-B (7), 952–960.
Bemben, D.A., Sherk, V.D., Ertl, W.J.J., Bemben, M.G., 2017. Acute bone changes after lower limb amputation resulting from traumatic injury. Osteoporos. Int 28 (7).
Branemark, P.I., 1983. Osseointegration and its experimental background. J. Prosthet. Dent 50 (3), 399–410.
Brånemark, R., Brånemark, P.-I., Rydevik, B., Myers, R.R., 2001. Osseointegration in skeletal reconstruction and rehabilitation. J. Rehabil. Res. Dev. 38, 175–181.
Brånemark, R., Berlin, Ö., Hagberg, K., Bergh, P., Gunterberg, B., Rydevik, B., 2014. A novel osseointegrated percutaneous prosthetic system for the treatment of patients with transfemoral amputation: a prospective study of 51 patients. Bone Jt. J. 96 (1), 106–113.
Clemente, F., et al., 2017. Touch and Hearing Mediate Osseoperception. Sci. Rep.
Dong, X.N., Guo, X.E., 2004. The dependence of transversely isotropic elasticity of human femoral cortical bone on porosity. J. Biomech.
Dowling, N.E., 2007. Mechanical Behavior of Materials: Engineering Methods for Deformation. Fracture and Fatigue 46 (12) third ed.
Dudek, N.L., Marks, M.B., Marshall, S.C., Chardon, J.P., 2005. Dermatologic conditions associated with use of a lower-extremity prosthesis. Arch. Phys. Med. Rehabil. 86 (4), 659–663.
Elder, M.A.C., Konvickova, S., Daniel, M., Horak, Z., 2017. Identification of the critical level of implantation of an osseointegrated prosthesis for above-knee amputees. Comput. Methods Biomech. Biomed. Eng. 1–8.
Eriksson, E., Brånemark, P.-I., 1994. Osseointegration from the perspective of the plastic surgeon. Plast. Reconstr. Surg. 93 (3), 626–637.

Frossard, L., 2019. Loading Characteristics Data Applied on Osseointegrated Implant by Transfemoral Bone-Anchored Prostheses Fitted with Basic Components during Daily Activities. Data Br.
Hagberg, K., Brånemark, R., 2001. Consequences of non-vascular trans-femoral amputation: a survey of quality of life, prosthetic use and problems. Prosthet. Orthot. Int. 25 (3), 186–194.
Hagberg, K., Häggström, E., Uden, M., Brånemark, R., 2005. Socket versus bone-anchored trans-femoral prostheses: hip range of motion and sitting comfort. Prosthet. Orthot. Int. 29 (2), 153–163.
Hagberg, K., Hansson, E., Brånemark, R., 2014. Outcome of percutaneous osseointegrated prostheses for patients with unilateral transfemoral amputation at two-year follow-up. Arch. Phys. Med. Rehabil. 95 (11), 2120–2127.
Hagberg, K., Ghassemi Jahani, S.-A., Kulbacka-Ortiz, K., Thomsen, P., Malchau, H., Reinholdt, C., 2020. A 15-year Follow-Up of Transfemoral Amputees with Bone-Anchored Transcutaneous Prostheses. Bone Joint J.
Häggström, E., Hagberg, K., Rydevik, B., Brånemark, R., 2013. Vibrotactile evaluation: osseointegrated versus socket-suspended transfemoral prostheses. J. Rehabil. Res. Dev. 50 (10), 1423–1434.
Helgason, B., Pálsson, H., Rúnarsson, T.P., Frossard, L., Viceconti, M., 2009. Risk of failure during gait for direct skeletal attachment of a femoral prosthesis: a finite element study. Med. Eng. Phys. 31 (5), 595–600.
Hoaglund, F.T., Jergesen, H.E., Wilson, L., Lamoreux, L.W., Roberts, R., 1983. Evaluation of Problems and Needs of Veteran Lower-Limb Amputees in the San Francisco Bay Area during the Period 1977-1980. J. Rehabil. R&D.
Hoyt, B.W., Walsh, S.A., Forsberg, J.A., 2020. Osseointegrated Prostheses for the Rehabilitation of Amputees (OPRA): Results and Clinical Perspective. Expert Rev. Med. Devices.
Jacobs, R., Brånemark, R., Olmarker, K., Rydevik, B., Van Steenberghe, D., Brånemark, P. I., 2000. Evaluation of the psychophysical detection threshold level for vibrotactile and pressure stimulation of prosthetic limbs using bone anchorage or soft tissue support. Prosthet. Orthot. Int. 24 (2), 133–142.
Lee, W.C.C., et al., 2007a. Kinetics of transfemoral amputees with osseointegrated fixation performing common activities of daily living. Clin. Biomech. 22 (6), 665–673.
Lee, W., et al., 2007b. Finite element modeling to aid in refining the rehabilitation of amputees using osseointegrated prostheses. Digit. Hum. Model. 4561, 655–658.
Legro, M.W., et al., 1999. Issues of importance reported by persons with lower limb amputations and prostheses. J. Rehabil. Res. Dev. 36 (3), 155–163.
Li, Y., Lindeque, B., 2018. Percutaneous osseointegrated prostheses for transfemoral amputations. Trending Orthop 41 (2), 75–81.
Meulenbelt, H.E.J., Geertzen, J.H.B., Jonkman, M.F., Dijkstraa, P.U., 2011. Skin problems of the stump in lower limb amputees: 2. influence on functioning in daily life. Acta Derm. Venereol.
Osseointegration. Merriam-Webster Medical Dictionary [Online]. Available: https://www.merriam-webster.com/medical/osseointegration. (Accessed March 2021).
Palmquist, A., Windahl, S.H., Norlindh, B., Brånemark, R., Thomsen, P., 2014. Retrieved bone-anchored percutaneous amputation prosthesis showing maintained osseointegration after 11 years-a case report. Acta Orthop. 85 (3), 442–445.
Prochor, P., Sajewicz, E., 2019a. A comparative analysis of standardised threads for use in implants for direct skeletal attachment of limb prosthesis: a finite element analysis. Appl. Bionics Biomechanics 2019, 1–10. February.
Prochor, P., Sajewicz, E., 2019b. The influence of geometry of implants for direct skeletal attachment of limb prosthesis on rehabilitation program and stress-shielding intensity. BioMed Res. Int.
Prochor, P., Frossard, L., Sajewicz, E., 2020. Effect of the material's stiffness on stress-shielding in osseointegrated implants for bone-anchored prostheses: a numerical analysis and initial benchmark data. Acta Bioeng. Biomech.
Reilly, D.T., Burstein, A.H., 1975. The elastic and ultimate properties of compact bone tissue. J. Biomech. 8 (6), 393–405.
Rubin, C.T., Lanyon, L.E., 1985. Regulation of bone mass by mechanical strain magnitude. Calcif. Tissue Int.
Sherk, V.D., Bemben, M.G., Bemben, D.A., 2008. BMD and bone geometry in transtibial and transfemoral amputees. J. Bone Miner. Res. 23 (9), 1449–1457.
Sherman, R., 1999. Utilization of prostheses among US veterans with traumatic amputation: a pilot survey. J. Rehabil. Res. Dev. 36 (2), 100–108.
Shigley, J.E., Mischke, C.R., Budynas, R.G., 2002. Shigley's Mechanical Engineering Design - 9th Ed., Vol. New York.
Stenlund, P., Trobos, M., Lausmaa, J., Brånemark, R., Thomsen, P., Palmquist, A., 2016. The effect of load on the bone-anchored amputation prostheses. J. Orthop. Res. 35 (5), 1113–1122.
Thesleff, A., Haggstrom, E., Tranberg, R., Zugner, R., Palmquist, A., Ortiz-Catalan, M., 2020. Loads at the Implant-Prosthesis Interface during Free and Aided Ambulation in Osseointegrated Transfemoral Prostheses. IEEE Trans. Med. Robot. Bionics.
Tomaszewski, P.K., Verdonschot, N., Bulstra, S.K., Verkerke, G.J., 2010a. A comparative finite-element analysis of bone failure and load transfer of osseointegrated prostheses fixations. Ann. Biomed. Eng.
Tomaszewski, P.K., Verdonschot, N., Bulstra, S.K., Verkerke, G.J., 2010b. A comparative finite-element analysis of bone failure and load transfer of osseointegrated prostheses fixations. Ann. Biomed. Eng. 38 (7), 2418–2427.
Tomaszewski, P.K., van Diest, M., Bulstra, S.K., Verdonschot, N., Verkerke, G.J., 2012a. Numerical analysis of an osseointegrated prosthesis fixation with reduced bone failure risk and periprosthetic bone loss. J. Biomech. 45 (11), 1875–1880.
Tomaszewski, P.K., Verdonschot, N., Bulstra, S.K., Rietman, J.S., Verkerke, G.J., 2012b. Simulated bone remodeling around two types of osseointegrated implants for direct fixation of upper-leg prostheses. J. Mech. Behav. Biomed. Mater.

Tranberg, R., Zügner, R., Kärrholm, J., 2011. Improvements in hip- and pelvic motion for patients with osseointegrated trans-femoral prostheses. Gait Posture 33 (2), 165–168.

Van de Meent, H., Hopman, M.T., Frölke, J.P., 2013. Walking ability and quality of life in subjects with transfemoral amputation: a comparison of osseointegration with socket prostheses. Arch. Phys. Med. Rehabil. 94 (11), 2174–2178.

Wolfram, U., Schwiedrzik, J., 2016. Post-yield and Failure Properties of Cortical Bone. Bonekey Rep.

Xu, W., Crocombe, a D., Hughes, S.C., 2000. Finite element analysis of bone stress and strain around a distal osseointegrated implant for prosthetic limb attachment. Proc. Inst. Mech. Eng. H. 214 (6), 595–602.

Xu, W., Xu, D.H., Crocombe, A.D., 2006. Three-dimensional finite element stress and strain analysis of a transfemoral osseointegration implant. Proc. Inst. Mech. Eng. Part H J. Eng. Med. 220 (6), 661–670.

Xu, D.H., Crocombe, A.D., Xu, W., 2016. Numerical evaluation of bone remodelling associated with trans-femoral osseointegration implant - a 68 month follow-up study. J. Biomech. 49 (3), 488–492.

Zioupos, P., Currey, J.D., 1998. Changes in the Stiffness, Strength, and Toughness of Human Cortical Bone with Age. Bone.